KiriInflate: Fabricating Cross-Scale Inflatables with Large Contraction and Tunable Stretchability for Tangible Interaction

Yue Yang
Zhejiang University
Hangzhou, China
yang_yue@zju.edu.cn

Chuang Chen
Zhejiang University
HangZhou, China
chenchuang@zju.edu.cn

Yulu Chen
University College London
London, United Kingdom
yulu.chen.23@ucl.ac.uk

Ge Gao
Zhejiang University
Hangzhou, China
gaoge.rita@gmail.com

Lei Ren
Zhejiang University
Hangzhou, China
renlei_design@zju.edu.cn

Bolan Yao
Zhejiang University
Hangzhou, China
bolan.yao@zju.edu.cn

Lingyun Sun
Zhejiang University
Hangzhou, China
sunly@zju.edu.cn

Ye Tao
Hangzhou City University
Hangzhou, China
taoye@hzcu.edu.cn

Guanyun Wang*
Zhejiang University
Hangzhou, China
guanyun@zju.edu.cn

Figure 1: Cross-scale primitive structures and applications of KiriInflate. (a) Comparison of cross-scale primitive KiriInflate; (b) Stretched state of a small-scale inflatable; (c) Eyelid lift assistive device for rehabilitation of ptosis; (d) Multi-mode Interactive game handle; (e) Breathable lamp. (Scale bar: 100 mm.)

Abstract

We present KiriInflate, a rapid, precise, and accessible fabrication method for creating stretchable inflatables with Kirigami structures. These inflatables, fabricated at multiple scales (from fingernail-sized to body-sized), exhibit rapid, large contraction upon inflation up to 83.5% and provide tunable stretchability. Our fabrication process leverages the electrostatic adhesion of plastic films and an off-the-shelf laser cutter to simultaneously cut and fuse the edges of inflatables, achieving ultra-narrow seals (< 0.125 mm). Our structural design enables versatile 3D morphing upon inflation and tunable stretch behavior, with experimental studies offering design guidelines for key geometric parameters. A series of applications, including an eyelid assistive device, a multi-mode game handle, a dynamic elbow brace, and breathable lamps, highlight its potential for diverse interaction in HCI.

CCS Concepts

• **Human-centered computing** → **Interactive systems and tools**.

Keywords

Inflatables, Cross-scale, Fabrication method, Tangible interaction

ACM Reference Format:
Yue Yang, Chuang Chen, Yulu Chen, Ge Gao, Lei Ren, Bolan Yao, Lingyun Sun, Ye Tao, and Guanyun Wang. 2025. KiriInflate: Fabricating Cross-Scale Inflatables with Large Contraction and Tunable Stretchability for Tangible Interaction. In *The 38th Annual ACM Symposium on User Interface Software and Technology (UIST '25), September 28–October 01, 2025, Busan, Republic of Korea.* ACM, New York, NY, USA, 15 pages. https://doi.org/10.1145/3746059.3747766

*Corresponding author

UIST '25, Busan, Republic of Korea

ACM ISBN 979-8-4007-2037-6/25/09
https://doi.org/10.1145/3746059.3747766

1 Introduction

Film-based inflatables have become a popular choice in soft robotics, wearable devices [8], and tangible interaction due to their deformability, accessibility, safety, and tunable force feedback [27, 43].

These structures are typically fabricated by thermally bonding non-stretchable polymer films to form sealed air chambers, with their deformation and mechanical behavior heavily dependent on geometric design. Beyond conventional heat-sealing patterns, integrating slits and kirigami-inspired cuts can significantly alter their inflated morphology and performance. For instance, kirigami actuators—composed of interconnected slits and channels—have gained attention in robotics for their enhanced contraction ratios and elastic stretchability [7]. Such structures hold promising yet underexplored potential for human-computer interaction (HCI), where dynamic shape-changing interfaces could enable novel tactile feedback, adaptive wearables, or deformable input devices.

However, fabricating inflatables with complex internal slits and fine channels remains challenging. Each slit edge requires precise thermal sealing, demanding high fabrication resolution in both cutting and heat welding. Existing approaches, such as AeroMorph [27] (custom CNC-based heat sealing), Millimorph [17] (hot-air sealing of pre-cut films), and Therms-up [6] (heat pressing through 3D printer), struggle with intricate internal slit patterns. Alternative methods, such as heating welding and cutting inflatables through laser cutter, produce wide welding seams (>0.5 mm) caused by defocused state of laser cutter, limiting their suitability for micro-scale slits and delicate channels [26]. Additionally, another technique that heat-presses film layers requires masking layers (e.g., release paper) that constrain material deformation. It is labor-intensive and prone to errors in alignment. These fabrication barriers hinder the exploration of inflatables with sophisticated internal slit structures, restricting their potential in HCI applications.

We introduce KiriInflate, a rapid, precise, and accessible method for creating inflatables with complex internal slits. (1) From the fabrication technique perspective, our approach leverages static cling adhesion between thin PE films and a standard laser cutter to simultaneously cut and heat weld complex edges of inflatables in a single step, achieving ultra-narrow and high-alignment of heat welding and cutting edges. We experiment with the parameter settings of the laser cutter for this new method to achieve both heat-welding only and heat-welding with cutting, accommodating to the varied material thickness for cross-scale fabrication. (2) From a structural design perspective, we expand the design space of inflatable actuators by introducing complex internal Kirigami-inspired slit geometries, made possible by our fabrication techniques. These designs enable versatile actuation behaviors with tunable stretchability. We systematically investigate the deformation characteristics of representative inflatable Kirigami structures, analyzing their active contraction ratios, passive stretch ranges, and output forces in relation to scale, geometric parameters, and material thickness. The application examples include an eyelid-lifting assistive wearable that conforms to natural blinking motions, a game controller integrating both inflation-driven haptic feedback and passive stretch interactions, and a shape-reconfigurable lamp. These examples showcase the potential of KiriInflate in dynamic conformability, shape reconfiguration, and haptic feedback for tangible interaction.

Compared to other inflatable fabrication techniques, our method has the following advantages:

High precision and resolution integrated cutting and welding. Cutting and sealing are performed simultaneously in a single laser pass, eliminating misalignment. This enables ultra-fine heat-welding edges (0.125 mm) and slit spacing down to 0.25 mm — significantly finer than typical methods [7, 26].

Cross-scale adaptability. Our method supports slit-based air channels from sub-millimeter to sub-meter widths. At small scales, it enables high inflation ratios using ultra-thin (thickness = 0.03 mm) materials and fine welding without release layers. At large scales, it accommodates thick multilayer films and reinforced welding edges, leveraging the large working area of laser cutters.

High efficiency and automation. The fabrication process is streamlined into a single laser pass without manual alignment of multiple layers, reducing labor and improving repeatability. Complex multilayer geometries are easily produced.

Low equipment barrier. The process works directly with standard laser cutters, requiring no hardware modifications. It relies on the natural electrostatic adhesion of thin PE films, avoiding external pressing attachment or vacuum devices.

Expanded design space for structural functionality. (a) Embedded kirigami architectures: Complex internal slit patterns (e.g., fractal cuts, gradient perforations) can be directly fabricated within sealed air chambers. (b) Multilayer pneumatic programmability: Single-step fabrication of stacked air chambers with multiple layers allows dynamic reconfiguration of deformation behavior through inflation in different layers.

Compared to existing works on inflatable shape-changing interface, the structure of KiriInflate has the following advantages:

Significant Active Contraction. Achieves significantly greater contraction than other pneumatic actuators (e.g., film inflatables without inner slits or McKibben fiber actuators [15]), with contraction reaching 83% of its original length after inflation and up to 97% compared to its pre-stretched state.

Enhanced Passive Stretchability with Tunable Compliance. When subjected to external forces, the inflated structure exhibits increased passive deformability. Its stretchable range can be customized through geometry parameters, and elastic response can be tuned by adjusting the internal air pressure.

High Programmability of Geometric and Mechanical Properties. Supports diverse deformation through the customization of slit patterns on 2D surfaces, enabling the rapid formation of stretchable 3D geometries with tailored mechanical properties.

In summary, the key contributions of this paper are as follows:

- A rapid, low-cost and highly accessible fabrication technique using a commodity laser cutter and the electrostatic adhesion of PE films to enable cutting and welding films in a single pass with ultra-narrow seams, thus fabricating cross-scale film inflatables (from finger-size to body size) with complex slit patterns.
- Versatile types of Kirigami inflatable structures with large contraction, different actuation behavior, and tunable stretchability based on the design of slits pattern, along with an online user document and assistive parametric geometry generators.
- A series of experimental analyses of tunable active contraction range, passive stretch range, and force behavior, which are related to the scale, geometry parameters, and material thicknesses.

- Four application examples showcase the potential of KiriInflate in dynamic conformability, shape reconfiguration, and haptic feedback for tangible interaction, including an eyelid-lifting assistive wearable that conforms to natural blinking motions, a dynamic elbow brace, a game controller integrating both inflation-driven haptic feedback and passive stretch interactions, and a series of shape-reconfigurable lamps.

2 Related Work

2.1 Inflatable Shape-changing Interfaces

Inflatable shape-changing interfaces driven by fluid pressure have been applied in fields such as soft robotics, furniture design [31, 38], architecture, wearables [18, 33, 45], transportation [25], and virtual reality [13, 37]. These systems are lightweight, low-cost, scalable, and easy to store, making them ideal for flexible, reconfigurable applications [20, 22]. Among inflatable structures, film-based inflatable structures leverage unreinforced thin films to make inflatables that deform through air pressure. Researchers in the fields of HCI, computer graphics and robotics have explored film-based inflatable structures to achieve bending and folding [27], bistable switching [43], and forming shape such as curved lines [34], curved surfaces [28, 30], and truss structure [29].

Kirigami-inspired inflatable structures, featuring sliced films, offer advantages such as high contraction ratios, tunable elasticity of stretch, and customizability via programmable cuts [7, 11, 32]. Chung et al. [7] introduced the concept of Inflatable Kirigami Actuators, fabricating these structures with a high contraction ratio using heat pressing and a masking layer. Building on their foundational designs, our work (1) expands range of scale (especially small scale, like fingernail-size) through our novel fabrication process, (2) achieves a higher contraction ratio through design optimizations like rounded slit ends, and (3) explores diverse and complex structures (e.g., multi-column array, multi-layer, curved patterns and 3D forms). These advances provide more versatile shape-changing effects and interactive feedback, enhancing the potential for HCI applications.

2.2 Kirigami Structure

Kirigami metamaterials, formed by embedding periodic cut patterns into thin sheets, are widely used for their superior stretchability and flexibility [35]. In robotics [14], Kirigami structures are primarily utilized as outer constraint layers for elastomers, modulating their deformation behaviors. In Human-Computer Interaction (HCI), kirigami structures have been applied in haptic feedback systems [4], stretchable 3D circuits [12, 42], and wearable devices that conform to body shapes and movements [3, 40].

Previous studies have investigated kirigami structures fabricated from various homogeneous materials, such as paper, wood, PE films, and metals - most of which are inherently rigid or non-elastic substrates. Researchers have systematically examined the passive deformation characteristics and elastic properties of these structures in relation to their geometric parameters [23]. Compared to Kirigami structures made from other materials, our work, KiriInflate, (1) introduces a pneumatically driven Kirigami actuation approach that enables rapid active contraction and dynamic morphological transformations. (2) Besides, unlike conventional materials, the stiffness, elasticity, and stretchability of inflatable kirigami structures can be dynamically tuned via internal air pressure. (3) In addition, the spatial distribution of air channels creates non-uniform mechanical properties, necessitating further exploration of shape-change dynamics and force response.

2.3 Fabrication of Film-based Inflatables

The fabrication of inflatable structures requires precise bonding of thermoplastic film layers, especially along complex cuts and edges that form air channels. Researchers have explored versatile, accessible fabrication methods for this purpose (Table 1). Specifically, heat-pressing film layers with internal masking layers is an accessible approach, but it struggles with alignment, which is labor-intensive, error-prone, and limited in resolution. The inner masking layer and wide edges also restrict the shape-changing capabilities of small-scale inflatables. Researchers have explored versatile automatic digital fabrication methods, such as using ultrasonic welding [11], customizing heat-sealing CNC systems [27], leveraging the heat nozzle of 3D printers [6], and heat welding using the defocused state of laser cutters [24, 26, 41]. However, the achievable sealing width remains relatively large (typically >400 μm). Furthermore, unlike thick, rigid materials that are easily stacked and welded by laser[21, 39], thin films require external pressure to ensure the intimate contact needed for creating narrow welds. More specialized laser welding techniques exist. For instance, the Ball Contour Process [1] employs a freely rotating glass ball for localized clamping, laser focusing, and height compensation. However, this process relies on sophisticated, custom-fabricated devices. Similarly, Millimorph [17] fabricates inflatables with micro channels using a customized CNC equipped with a needle that emits hot air to seal pre-cut layers. Nevertheless, this approach still requires manual trimming of external contours, as drag knife tools risk scratching the chuck. Consequently, most existing fabrication methods rely on complex, specialized equipment to ensure proper film alignment and layer contact during the bonding process, which present additional challenges for their widespread adoption and scalability.

We propose a highly accessible method that synchronizes the cutting and heat sealing of electrostatically bonded film layers with high resolution. Our approach leverages standard laser cutters without hardware modification, eliminating the need for tedious manual alignment or sophisticated custom devices. This streamlined process simplifies operation and enables the high-precision fabrication of complex internal structures with ultra-narrow seals (min. 0.04 mm). It allows rapid prototyping with varied film layers and thicknesses, expanding the design space for soft and responsive inflatables.

3 Overview of KiriInflate

3.1 Fabrication Technique of KiriInflate

KiriInflate introduces a rapid, precise, and accessible method for creating inflatables with complex internal slits Below we introduce the novel pipeline and fabrictaion setting supporting cross-scale fabrication.

Table 1: Comparison of Representative Methods for Inflatable Fabrication.

Project	Method	Machine	Efficiency	Inner Cuts	Seal Width
Therms-up [6]	Heat press sealing	3D printer	High	✗	0.4 mm
AeroMorph [27]	Heat drawing	Customized CNC	High	✗	≈6.35 mm
AccordionFab [41]	Heat welding and cutting	Laser cutter with attachment	High	N/A	N/A
Inflatable Kirigami [7]	Heat pressing with masking layer	Laser cutter + heat press	Low (manual)	✓	1 mm
Pneumatic Origami [26]	Laser welding	Laser cutter + vent	High	N/A	≈0.92 mm
Millimorph [17]	Hot air sealing	Customized CNC	High	✗	0.25 mm
Weld n' cut [11]	Ultra-sonic welding	Customized CNC	High	✓	4 mm
Our Work★	Heat welding and cutting	Laser cutter	Ultra high	✓	0.125 mm

3.1.1 Pipeline. A plastic film material, PE, that can automatically adhere to itself due to electrostatic attraction is selected. By utilizing the electrostatic attraction between two layers of film, the laser cutting machine can simultaneously cut and heat-seal the edges of the inflatable during a single pass.

- **Step 1** (Figure 2a): Prepare a double-layer plastic film that automatically adheres to itself due to electrostatic attraction (for example, use two or more layers of PE film with electrostatic adhesive).
- **Step 2** (Figure 2b): The laser cutting machine runs along the path, simultaneously cutting and heat-sealing the edges of the inflatable. Alternatively, a lower power setting can be used to only heat-seal along the path without cutting. Due to the electrostatic attraction between the two layers of film, they adhere firmly, enabling high-quality heat sealing after the laser passes.
- **Step 3** (Figure 2c): The inflatable quickly shrinks and deforms upon inflation. Because there are some cut seams, the inflated structure exhibits greater tensile elasticity.

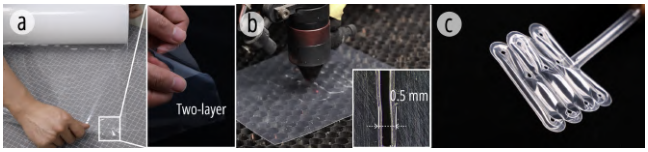

Figure 2: The fabrication pipeline of KiriInflate.

3.1.2 Cross-Scale Fabrication Parameter. In the fabrication of inflatables, laser cutting technology provides two alternative methods: (1) simultaneous heat welding and cutting; (2) heat welding without cutting. The fabrication parameters vary depending on the thickness and scale of the inflatables. This section outlines the parameters for both methods and provides experimental data for reference. The laser cutter we used in the demonstration is Laserbox 2.0 (MLP-K503-40W).

For the simultaneous heat welding and cutting method, the relevant parameters are shown in Table 2. Cylindrical inflatables with dimensions of 15 mm × 60 mm and single-layer material thicknesses of 0.03 mm, 0.05 mm, 0.07 mm, 0.1 mm (two-layer 5 mm), 0.14 mm (two-layer 7 mm), and 0.2 mm (four-layer 5 mm) were tested. Laser power and speed combinations were optimized through experiments, and the sealed inflatables were inflated in water to check for leaks.

For thinner materials, high power can achieve both heat welding and cutting simultaneously. However, due to the thermal shrinkage of the PE film, excessive power can cause the cut seams to widen, which may impact the width of the airway. While this difference is not significant in some cases, it becomes particularly important for small-scale inflatables. Additionally, we found that for materials thicker than 0.1 mm, even when using higher power, achieving perfect cutting is difficult. The cut material may exhibit filament-like adhesions, likely due to the thickness of the material, which may adhere during the cooling process after cutting. However, this does not affect the air tightness of inflatables.

Table 2: Parameters for Heat Welding and Cutting.

Thickness (mm)	0.03	0.05	0.07	0.1	0.14	0.2
Power (%)	27	29	33	50	80	80
Focal Length (mm)	0.1	0.1	0.1	0.2	0.3	0.4
Speed (m/s)	50	50	50	50	42	35

For the heat welding-only method, the test samples and procedures are the same as described above. The parameters for simultaneous heat welding and cutting are shown in Table 3. This method ensures that all layers of material are effectively heat-sealed without cutting through.

Table 3: Recommended Parameters for Heat Welding-Only.

Thickness (mm)	0.03	0.05	0.07	0.1	0.14	0.2
Power (%)	21	22	23	22	24	30
Focal Length (mm)	0.1	0.1	0.1	0.2	0.3	0.4
Speed (m/s)	50	50	50	50	50	50

In addition to the two methods described above, the width of the heat-sealed edge is a critical design parameter that directly influences the sealability of the inflatables, mechanical strength,

and durability. For inflatables made from thicker materials, a wider heat-sealed edge is typically required to ensure adequate fusion depth, withstand hoop stress during inflation, and prevent cracking at the seal. In our experiments, we tested the same inflatable samples with different seam widths: 0.5 mm, 1.0 mm, and 1.5 mm. Using an orthogonal combination experiment, each group was inflated and pressurized, and the maximum pressure capacity was recorded. The reference heat-sealed edge widths are summarized in Table 4. We found the use of 0.2 mm materials resulted in unstable performance, such as difficulty in cutting through the material in a single pass, leading to inconsistent pressure resistance.

Table 4: Pressure Resistance (PSI) vs. Material Thickness and Edge Sealing Width.

Edge Width (mm)	Material Thickness (mm)					
	0.03	0.05	0.07	0.10	0.14	0.20
0.5	3	4.5	10	14	24	24.5
1.0	4	5.5	14	17	25	22
1.5	6	7.5	16	19	26	30

3.2 Basic Mechanism and Structure of KiriInflate

The shape and mechanical behavior of KiriInflate are primarily determined by the heat-sealing traces and slits [28].

Heat Sealing Traces: Initially, when air is pumped into the channels, their expansion is constrained by the surrounding sealed regions. This confinement forces the material between the channels to contract sideways, which causes the cross-sectional shape of each channel to transform from flat to cylindrical [10]. As a result, the surface curvature of the structure changes, manifesting as dome-like, arched, or wavy forms. This process reconfigures the entire sheet from a flat 2D surface into a more compact 3D structure.

Slits: In addition to the heat-sealing pattern, the kirigami-style slits play a crucial role in shaping the structural behavior. While the slits do not alter the internal pressure distribution of individual air channels, they effectively segment the continuous film into truss-like units. This segmentation removes movement restrictions between adjacent channels, allowing them to slide, rotate, or even overlap during inflation. Consequently, the overall contraction of the structure is significantly enhanced. Figure 3 demonstrates the comparison of inflatables with and without slits. Moreover, when the slits are arranged in parallel, they function as hinges, enabling the air-filled columns to rotate around their endpoints, which further increases the structure's stretchability.

Together, the combination of heat sealing and slits gives the structure tunable mechanical behavior:

- **Active contraction (inflation-driven):** Air pressure generates strong driving forces for contraction. The degree of shrinkage is governed by both the internal pressure and the geometry of the kirigami cuts.
- **Passive stretching (externally applied force):** After inflation, the structure resists deformation and behaves like a soft spring. This elastic resistance can be tuned by adjusting the air pressure.

Furthermore, the structure exhibits three distinct states based on the inflation process:

- **Uninflated:** In this state, the kirigami cuts allow for large, easy stretching, with the structure remaining soft and highly flexible.
- **Inflating:** During this phase, air pressure drives the structure to contract. The deformation pattern is shaped by both the heat-seal layout and the kirigami cut design.
- **Inflated:** Once fully inflated, the structure maintains a compact, contracted form. While it becomes stiffer, it remains stretchable, and its resistance to stretching increases with air pressure.

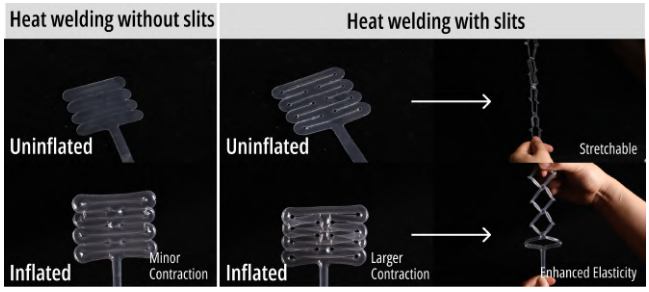

Figure 3: Comparison of inflatables without and with Kirigami slits. The inflatable with Kirigami slits exhibits large contraction after inflation. It also offers a greater stretchable range with tunable elasticity.

3.3 Design Space of KiriInflate

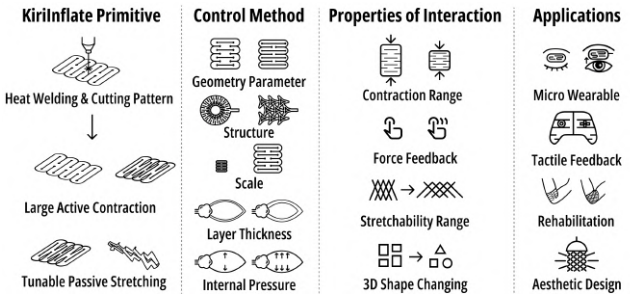

Figure 4: Overview and Design space of KiriInflate.

We are motivated to harness the benefits of Kirigami slits structures in inflatables which opens up a new design space for creating inflatables with significant active contraction or shape change, enhanced stretchability with tunable elasticity. We present a diagram described in Figure 4 to map out the design space of KiriInflate:

1) ***Structure.*** KiriInflate introduces heat welding and slits structure primitives to versatile structure, such as multi column array, uneven distribution, curved slits patterns, and multilayer. These structures achieve versatile actuated shapes with stretchability.

2) ***Scale.*** The flexibility in size allows for interaction across diverse scales, from sub-millimeter to sub-meter scale (Figure 5).

3) ***Geometry parameter.*** The geometric parameters of the internal heat-welding and slits patterns control the range of motion, including the actuated contraction, passive stretchable range, and elastic force feedback.

4) ***Material thickness and internal pressure.*** The fabrication technique supports multi-layers with different thicknesses. Adjustments of internal pressure can tune the elasticity behavior.

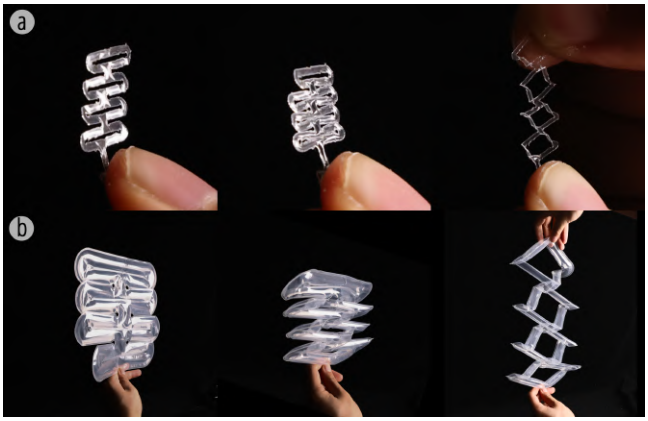

Figure 5: Cross-scale structures with single air column range from (a) 1.5 mm and (b) 30 mm.

The main advantages of KiriInflate structure are that they have large-range active contraction once inflated, and the elastic force is passively enhanced at the same time. As shown in Figure 6a, the KiriInflate with each air channel width of 15 mm can quickly retract against the gravity of a 100 g weight. Figure 6b and Figure 6c show the size difference of the KiriInflate between the pre-stretched state and the inflated, contracted state.

In our applications, we showcase the potential of our work in dynamic conformability, shape reconfiguration, and haptic feedback for tangible interaction. Examples include an eyelid-lifting assistive wearable that conforms to natural blinking motions, a game controller integrating both inflation-driven haptic feedback and passive stretch interactions, and a shape-reconfigurable lamp.

3.4 Structure Design of KiriInflate

Through the design of heat-welding and cutting patterns, we present a series of inflatable structures incorporating kirigami patterns. These inflatables demonstrate versatile performance when inflated and exhibit varying degrees of stretchability.

3.4.1 Primitives. As shown in Figure 7, the Kirigami-inspired inflatable structures that commonly emerges from the current study feature simple straight slits, which provide a certain degree of stretchability and contractility [7].

KiriInflate builds upon this structure with several key optimizations. First, through introducing micro circular ends at the tips of the slits inspired by [5], the effective length of each cut is extended, allowing for a greater range of stretch. Additionally, the rounded

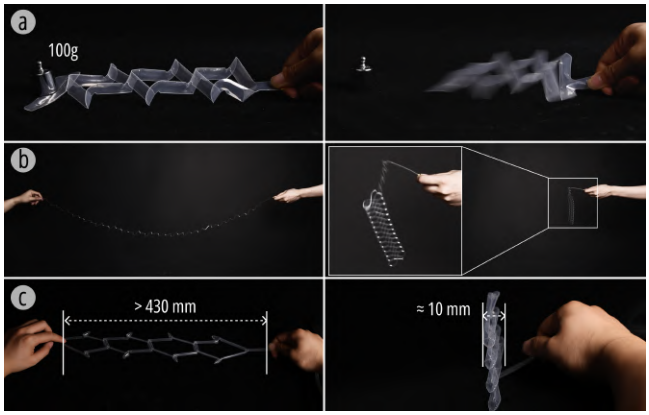

Figure 6: Large contraction effect of KiriInflate. (a) The KiriInflate with a 15 mm air channel width can rapidly contract after inflation, overcoming the gravity of a 100 g weight. (b) and (c) show that KiriInflates of two different scales can both contract quickly and significantly once inflated.

ends promote better overlapping of the structure during contraction, thereby enhancing its overall compressibility. Furthermore, we redesigned the original rectangular corners of the internal air channels into smooth arcs. This modification reduces stress concentration at sharp corners, which is a common cause of airbag rupture, and thereby significantly improves the stability of airtightness.

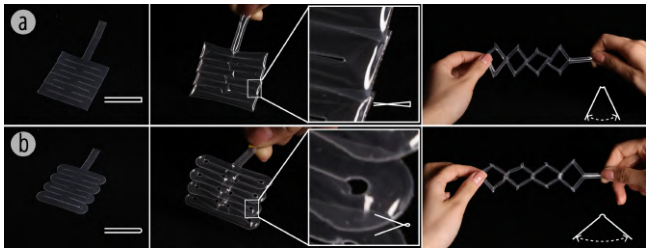

Figure 7: Primitives. (a) is Conventional Kirigami-inspired inflatable and (b) is our Optimized KiriInflate.

3.4.2 Array. By systematically arranging primitive Kirigami and varying the connection pattern between the two adjacent units, three distinct types of elastic curved surfaces with differing mechanical behaviors can be achieved (as shown in Figure 8). These variations of connections may also be interpreted as differing degrees of surface perforation, allowing amounts of compressible space during structural contraction.

Fully Connected (Figure 8a): Adjacent kirigami columns are completely overlapped, resembling a monolithic surface patterned with continuous kirigami cuts. The interlocking segments impose mutual constraints, resulting in relatively limited contraction but enhanced elastic restoring force.

Partially Connected (Figure 8b): This intermediate design features partial overlap between adjacent columns, producing considerable contraction along with visible overlapping effects reminiscent of woven textiles. However, its elastic restoring force is comparatively reduced.

Disconnected (Figure 8c): Each kirigami column is structurally independent, connected only by a topmost air channel. Due to the absence of lateral constraints, this design permits the greatest degree of contraction with minimal elastic response.

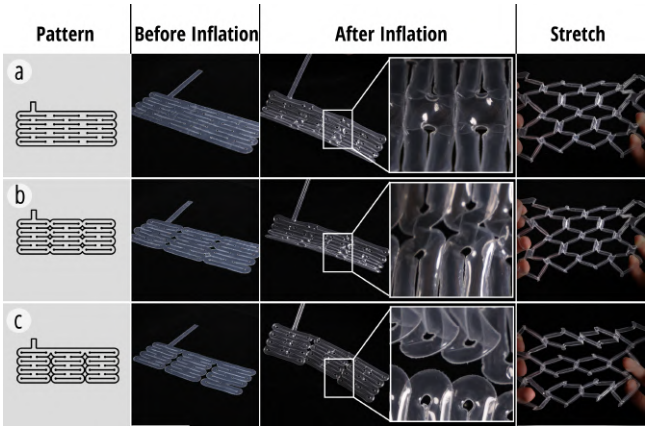

Figure 8: Array: (a) Fully Connected; (b) Partially Connected; (c) Disconnected.

3.4.3 Nonuniform Channel. The uneven distribution of Kirigami slits within an inflatable structure can lead to variations in air channel dimensions, which in turn induce uneven internal stress and result in unique deformation behaviors.

Asymmetric Side Slit (Figure 9a): When the slits on the left side are shorter than those on the right, the air channel on the left becomes wider than that on the right. Upon inflation, the left side of the kirigami structure contracts less readily than the right, causing the entire actuator to bend laterally toward the right.

Vertically Graded (Figure 9b): Given that the width of air channels significantly influences the stretchability of KiriInflate, designing a gradient in channel width enables the actuator to exhibit graded elasticity. During interaction, this allows the slits to open sequentially. Morphologically, this gradient also induces a curling deformation of the airbag toward one side.

Zoned (Figure 9c): Using a heat-weld process without cutting-through, a single Kirigami layer can be divided into two separately controlled segments, each with independent inlets while maintaining mechanical interaction. The left and right air channels are not interconnected. Under fixed-length conditions, inflating one side causes it to contract, which in turn mechanically pulls the other side into extension.

3.4.4 Curved Pattern. Building upon conventional straight-line Kirigami slits, we developed several curved cut variants to explore new deformation behaviors.

Parallel Wavy Line Surface (Figure 10a): This kirigami pattern remains planar after inflation and retains effective contraction and

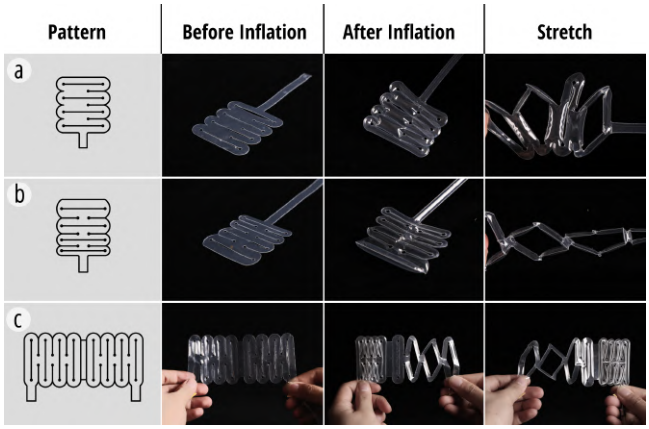

Figure 9: Nonuniform Channel: (a) Asymmetric Side Slit, (b) Vertically Graded, (c) Zoned.

extension capabilities. A similar zigzag-shaped indentations has been studied by Tian Gao et al., where it resulted in complex 3D deformations [10]. However, as discussed earlier, the KiriInflate design removes movement restrictions at the cut sites for a plan, which explains the flatness of the cutting geometry despite its curvature.

Tween Curve Surface and Mirrored Tween Curve Surface (Figure 10b): This configuration generates a curved surface upon inflation, with the bending direction perpendicular to the orientation of the air channels. We hypothesize that this occurs due to differential contraction along the direction orthogonal to the air channels; that is, variations in local contraction across the channel width create curvature in the inflated structure.

Bulging Waveform Surface (Figure 10c): By densely arranging interlocking Single Bulging Wave Line 2 curve cuts across a surface, the structure can bend into a continuous 3D surface upon inflation. The geometry enables the actuator to bend along the direction of the embedded air channels.

Single Bulging Wave Line (Figure 10d): When extracted from the densely tiled arrangement, this individual curved element could still bend autonomously along the direction of the air channel upon inflation. Notably, it consistently bends toward the side that was closer to the laser head during thermal bonding—a phenomenon similar to that observed in aeroMorph [27]. Furthermore, by controlling the width ratio between the wide and narrow sections of the air channel, the curvature can be tuned: the greater the width difference, the larger the resulting bend.

Single Wavy Line (Figure 10e): Upon inflation, this loosely arranged wavy line contracts and retracts, generating a tightening effect akin to that of crocheted yarn being drawn taut.

3.4.5 Multi-layers. Based on the experimental findings regarding material thickness and its pressure-bearing capacity, we observe that thicker layers deform less under the same internal pressure. Furthermore, we demonstrate that selective inflation of different layers within a multilayer KiriInflate can induce diverse deformation modes.

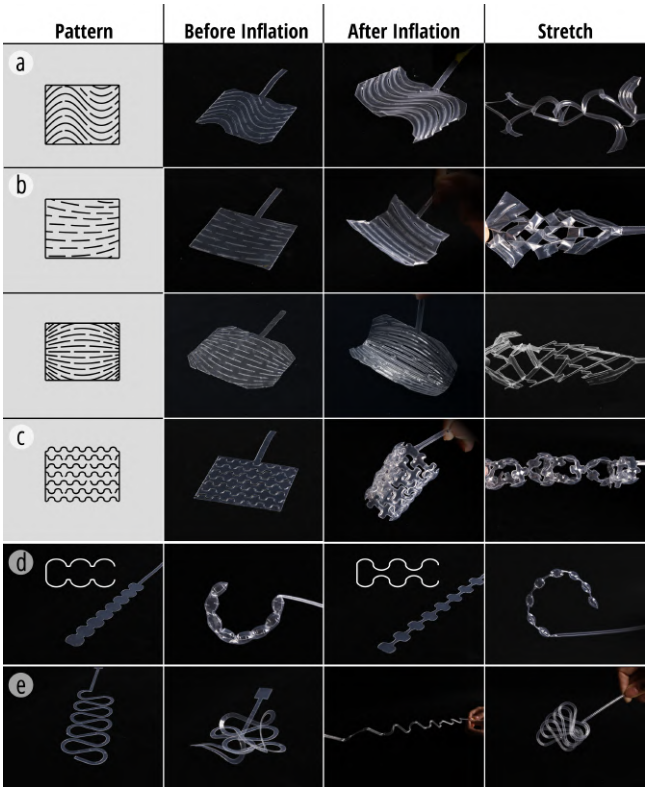

Figure 10: Curved Pattern: (a) Parallel Wavy Line Surface, (b) Tween Curve Surface and Mirrored Tween Curve Surface, (c) Bulging Waveform Surface, (d) Single Bulging Wave Line, (e) Single Wavy Line.

Multilayer "Bulging Waveform Surface" (Figure 11a): The basic "Bulging Waveform Surface" admits the characteristic of bending to one side. In multilayer versions of this structure, we observed that when the number of membrane layers is asymmetrical, the structure preferentially bends toward the side with fewer layers. Moreover, the greater the asymmetry between the selected layers, the greater the inflation deformation bending curvature.

Multilayer, Multi-channel Kirigami (Figure 11b): We designed a multilayer kirigami actuator with its axis of symmetry heat welded. This configuration enables programmable bending deformation in six distinct directions: forward, front-left, front-right, backward, back-left, and back-right. The mechanism for side bending in this structure is similar to the "Asymmetric Side Slit" case discussed earlier.

3.4.6 3D Surface with Stretchability. In addition to the unidirectional bending surfaces, we also propose a rapid method for generating complex, elastic surfaces with diverse deformation capabilities:

Radial Slit (Figure 12a): This design inspired by [19] transitions from a 2D toroidal (donut-shaped) form to a 3D cylindrical shape upon inflation. The kirigami pattern endows the structure with adaptability to cylindrical or spherical geometries of different diameters, making it suitable for integration with deformable biological

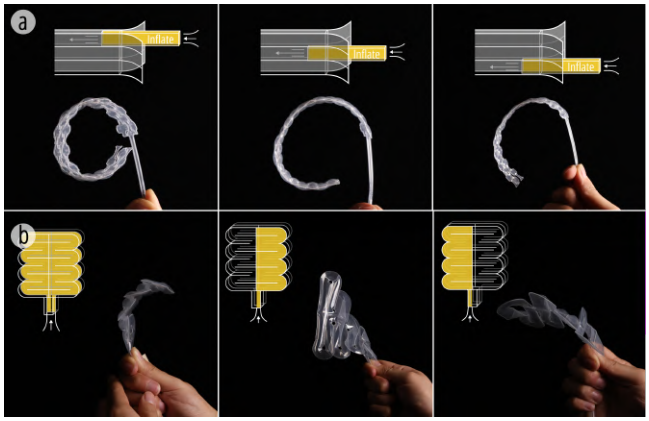

Figure 11: Multi-layers. (a) As the inflation port moves towards the middle layer, the thickness difference between the two sides of the KiriInflate structure decreases, and the bending curvature gradually decreases. (b) To inflate the innermost layer, the KiriInflate is bent forwards; to inflate the left airway of the outermost layer, the KiriInflate is bent backwards to the left; to inflate the right airway of the outermost layer, the KiriInflate is bent backwards to the right.

tissues such as the upper and lower limbs, fingers, abdomen, or even the heart.

Y-shaped Slit (Figure 12b): This structure transforms into a highly elastic arched shape upon inflation. Its geometry is particularly suitable for wearable applications around joint regions, where it conforms closely to the body while providing impact protection without restricting joint mobility.

Concentric Circular Slit (Figure 12c): A kirigami pattern arranged along concentric circles with varying diameters produces a saddle-like geometry upon inflation, characterized by high elasticity and negative Gaussian curvature. This configuration may be well-suited for applications requiring surface adaptability in multiple directions—such as soft robotic skins, adaptive seating interfaces, or wearable exoskeletal supports for complex anatomical regions.

3.4.7 Dynamic Hollow Pattern. As illustrated in Figure 12d and Figure 12e, by perforating a curved surface with a densely packed pattern of Triangular and Quadrilateral Star Channel cuts, an elastic surface with controllable porosity can be obtained. Upon inflation, increasing the internal pressure causes each individual star-shaped unit to contract, thereby reducing the size of the surface pores. This design enables dynamic modulation of porosity in response to pressure changes, offering potential applications in fields such as tunable filtration, adaptive ventilation, or morphing architectural skins.

4 Tunable Motion and Elasticity

Various parameters can affect the performance of the inflatable kirigami structure. Currently, there is no standardized design method for creating inflatables with these characteristics. In this section, we conduct a series of tests to verify that inflatable scale, width, slit width, and material thickness can be adjusted as variables to

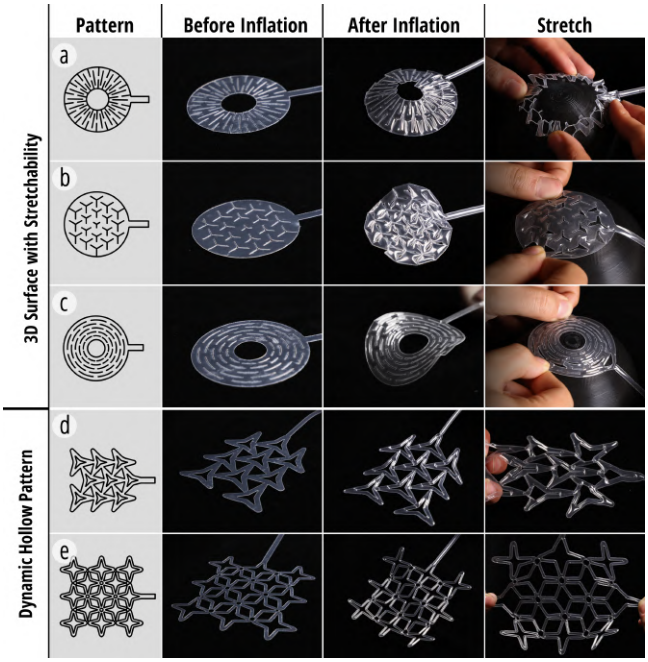

Figure 12: 3D Structure with Stretchability and Dynamic Hollow: (a) Radial Slit, (b) Y-shaped Slits, (c) Concentric Circular Slit, (d) Triangular Star Channel, (e) Quadrilateral Star Channel.

control the inflation contraction rate, contraction force, and tensile force required to achieve the maximum size of KiriInflate (Figure 13).

During the tests, the inflatable contracted after inflation, and as each unit structure stacked, we measured the projection distance after stacking to determine the contraction distance, subsequently calculating the contraction ratio λ. To measure the contraction force F_c, the inflatable was fixed in its uninflated and unstretched position, and the contraction force was measured using a force gauge after inflation. For the tensile force, we first measured the maximum stretchable distance $L_{\max}$of the inflatable when uninflated. Then, after inflation, the inflatable was stretched to its maximum distance, and the tensile force F_t was measured.

All tests were performed with three samples, and the air pressure in the inflatables was maintained at 50 kPa using a pressure regulator.

4.1 Scale

We compared the performance of inflatables with different sizes (ranging from a single column width of 2 mm to 17 mm, increasing in increments of 3 mm). To simulate real-world conditions, we applied a material thickness scheme that was adjusted according to the size of the inflatable: larger inflatables were made with thicker materials, while smaller ones were made with thinner materials.

As shown in Figure 14, the test results indicate a significant positive correlation between the size of the inflatable and its performance. Specifically, the maximum stretchable length increases significantly as the size grows, with the largest inflatable (17 mm)

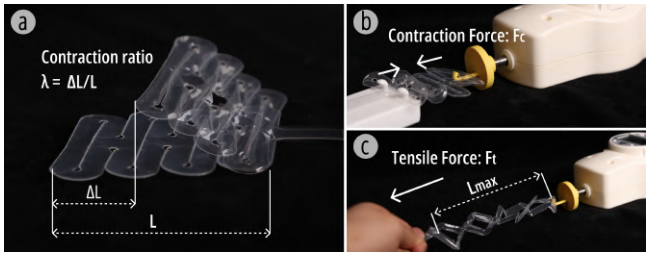

Figure 13: The experimental setup tests the adjustment of (a) contraction ratio, (b) contraction force, and (c) tensile force for KiriInflate.

reaching a maximum stretch length of 366 mm. Both the contraction force and tensile force increase in parallel, with the largest sample requiring 6.37 N of force to achieve maximum stretch.

The contraction ratio generally increases with the size of the inflatable. When the single column width reaches 14 mm, the maximum contraction ratio can reach 69.76%. This phenomenon is likely due to the fact that the sealing width during manufacturing did not scale proportionally with the size of the inflatable, causing the smaller inflatables to be more affected by fabrication process. However, when the sample size reached 17 mm, the contraction ratio decreases to 59.5%. We hypothesize that this is due to the increased resistance to deformation caused by the thicker material: the thicker the material, the greater the internal stress that needs to be overcome during contraction, thus reducing the contraction ratio.

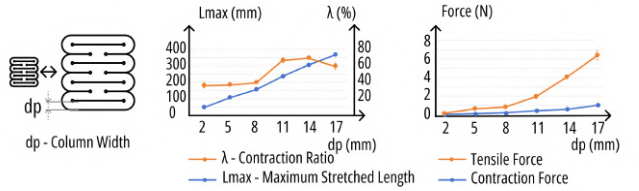

Figure 14: Experimental results of the performance of inflatables with different sizes.

4.2 Geometry Parameter

To assess the impact of inflatable width on its performance, we conducted tests under fixed structural parameters (single column width of 8 mm and material thickness of 0.07 mm) while varying the total inflatable width (20-160 mm, with increments of 20 mm). As shown in Figure 15a, when the inflatable width exceeds 100 mm, the truss structure upon inflation exhibits near-complete vertical overlap, with the contraction ratio reaching its maximum value of 83.5%. Additionally, the maximum stretchable length increases substantially with width, with the largest sample (160 mm wide) achieving a maximum stretch length of 433 mm. However, both the contraction and tensile forces exhibit a decreasing trend.

Similarly, we controlled the silt overlap distance to examine its impact on the inflatable (Figure 15b). Under fixed structural parameters (single column width of 8 mm, material thickness of 0.07

mm, and inflatable width of 64 mm), we varied the silt overlap distance (from 8 mm to 2 mm, with increments of 2 mm). Our findings reveal that reducing the overlap distance significantly enhances both the contraction ratio and stretchability, while corresponding contraction and tensile forces decrease.

This trend follows a mechanism similar to that observed with width: reducing the overlap distance decreases the constraint between adjacent truss units, reducing the friction and constraint forces that need to be overcome during deformation, thereby improving the deformability of the structure. However, this improvement comes at the cost of mechanical strength.

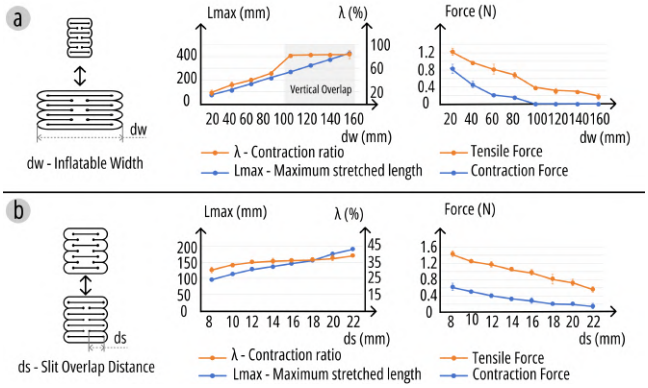

Figure 15: Experimental results of the performance of inflatables with different (a) inflatable widths and (b) slit widths.

4.3 Material thickness

To investigate the effect of material thickness on the performance of inflatables, we prepared experimental samples with different thicknesses under fixed structural parameters (single column width of 8 mm, total width of 64 mm, and slit overlap distance of 18 mm). The material thicknesses used in the experiment were 0.03 mm, 0.05 mm, 0.07 mm, 0.1 mm, 0.14 mm, and 0.2 mm.

As shown in Figure 16, the test results indicate that variations in material thickness significantly affect the contraction ratio and mechanical properties.

As the material thickness decreases, the contraction ratio of the inflatable shows a clear increasing trend, reaching up to 46.45%. This phenomenon is mainly due to two factors: thinner materials experience lower internal stress during contraction, allowing for a higher contraction ratio, while thicker materials hinder the complete overlap of the air column truss structure, limiting the maximum contraction ratio.

However, the reduction in material thickness is also accompanied by a decrease in mechanical performance, as indicated by a reduction in both contraction and tensile forces. This is due to the lower stiffness of thinner materials, which are more prone to elastic deformation under stress, thus weakening the overall load-bearing capacity.

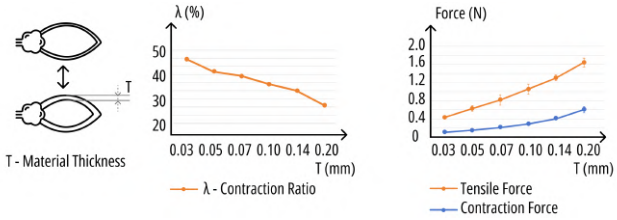

Figure 16: Experimental results of the performance of inflatables with different material thicknesses.

4.4 Performance of Complex Structures and Design Assistance

Beyond the primitive unit, we also investigated how scale, geometry, and material thickness influence the diverse structures presented in Section 3.4 (e.g., Arrays, Curved Patterns, 3D forms). Due to the complex, multi-directional mechanical responses of these shapes, our evaluation focused on qualitatively analyzing their morphological transformations under varied parameters. Our experiments confirm that these parameters have a consistent and predictable influence on the deformation of complex structures, similar to their effects on the primitive unit. We also documented and analyzed anomalous behaviors observed during testing. To support these findings and facilitate replication, we developed a comprehensive web-based user document[1] that provides detailed observational data, explanations, and images for each structure (Figure 17). Furthermore, we offer a series of online parametric geometry generators on the website, allowing users to adjust key parameters and directly export fabrication-ready DXF files. These tools, built with Rhinoceros[2], Grasshopper[3], and ShapeDiver[4], lowers the barrier for other researchers and makers to build upon our work.

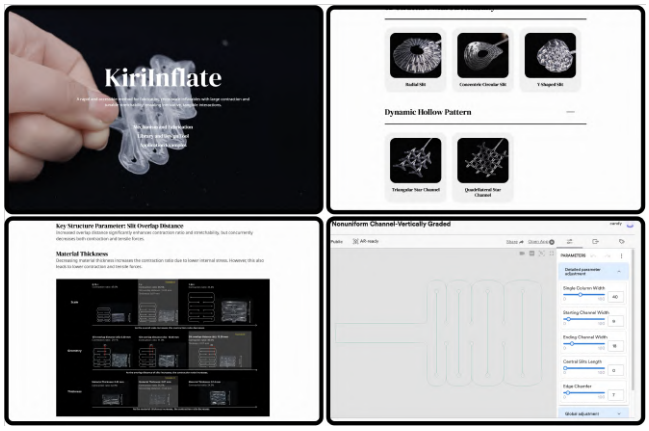

Figure 17: KiriInflate web document, featuring parametric design generators on each structure page.

[1]https://kiriinflate.github.io/
[2]https://www.rhino3d.com/
[3]https://www.grasshopper3d.com/
[4]https://www.shapediver.com/

5 Application Example

5.1 Conformable Eyelid Assistive Device

Ptosis is often caused by neuromuscular disorders, and patients are often unable to open their eyes properly due to weakness of the eyelid muscles [9]. In most non-severe cases of ptosis, although the ability to open the eyes is impaired, the neuromuscular complex that controls eyelid closure remains intact. For such conditions, it is possible to use an artificial levator muscle to assist in restoring normal eyelid elevation. Current non-invasive assistive tools, such as eyelid crutches and kinesiology tapes, provide eyelid support but hinder natural blinking. We have designed a rehabilitation assistive device (Figure 18) that provides auxiliary lifting force to the eyelid while allowing natural blinking movements.

Before inflation, the kirigami structure stretches but exerts minimal force, thus not interfering with eyelid closure. Upon inflation, the inflatable contracts, increasing the lifting force and helping to raise the eyelid, allowing the patient to open their eyes more easily. At the same time, the patient only needs to exert a small amount of effort to blink. This means the device does not interfere with normal blinking, and during the blinking process, it also provides resistance training that helps strengthen the eyelid muscles.

For attachment, the actuator can be secured to the eyelid using medical-grade skin adhesive or eyelash glue. The material we used, Polyethylene (PE), is recognized as a promising polymer for wearables due to its high infrared transparency and tunable visible opacity [2]. Comprehensive studies on long-term wearability and comfort would be a necessary step toward future clinical application.

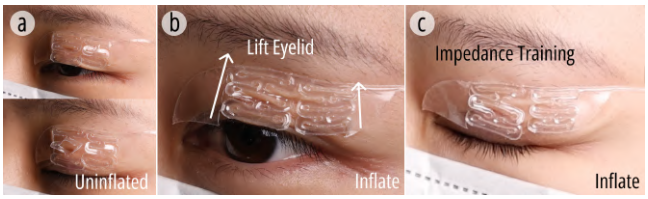

Figure 18: (a) Eyelid assistive device that does not interfere with normal eye movement when uninflated, and (b) provides eyelid lifting support while (c) allowing natural blinking and offering resistance training when inflated.

5.2 Dynamic Elbow Brace

We have developed an adjustable pressure elbow brace that automatically contracts after inflation (Figure 19). Unlike traditional bandage braces, this device allows users to adjust the pressure on the elbow by regulating the air pressure, enabling dynamic pressure adjustment and eliminating the need for frequent donning and doffing. Additionally, dynamic compression can be achieved through rapid inflation and deflation. Compared to traditional rigid or inflatable braces, the kirigami structure ensures that the brace does not restrict the elbow's range of motion, allowing for free bending. This dynamically adjustable brace can real-time adjust pressure during sports training, balancing protection and performance, and effectively preventing overuse injuries during prolonged use, making it highly applicable.

Figure 19: (a-b) Adjustable pressure elbow brace that automatically contracts upon inflation, (c) while allowing for unrestricted bending.

5.3 Multi-mode Game Handle

We developed an interactive game handle integrated with tactile feedback and sensing functions using KiriInflate (Figure 20). The handle features a multi-layer structural design, primarily consisting of three independent air chambers: the upper left chamber, the upper right chamber, and the lower main chamber. When the game requires a leftward action, the upper left chamber inflates, causing lateral contraction on the left side. This tactile feedback prompts the user to press the left function button, which is equipped with a graphene conductive coating to enable touch sensing functionality. The rightward action feedback is achieved with the same principle using the right chamber. The lower main chamber serves a dual function: upon inflation, it facilitates overall contraction movement of the controller, and when stretched, it activates the sensing function. This sensing function, implemented through pre-installed graphene conductive circuits, detects the displacement caused by the stretching of the controller, thereby simulating actions such as bullet firing in the game.

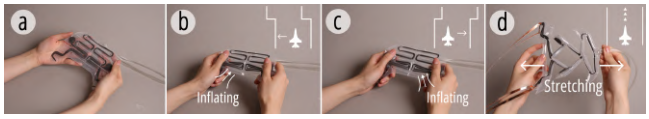

Figure 20: (a) Interactive game handle with three air chambers: (b) upper left, (c) upper right, and (d) lower main, featuring tactile feedback and sensing functions.

5.4 Breathable Lamps

We have developed some inflatable, shape-shifting lamps (Figure 21). In their uninflated state, the lamps naturally hangs down under the influence of gravity, taking on a soft, pre-stretched form that creates a gentle, tranquil atmosphere. Upon inflation, the lamps actively contracts, transforming into a structurally defined three-dimensional shape, offering a striking visual contrast. This transformation allows users to intuitively perceive the "breathing" and "life" of the lamps, with the dynamic shift in form not only reflecting the interaction between structure and material, but also emphasizing the dynamic relationship between the user and the product. The KiriInflate imbues the lamps with unique aesthetic value and sensory experience.

The inflating method of the lamp holds great potential for future exploration. By injecting a low-boiling liquid into the inflate, it automatically inflates and changes shape when the lamp is turned on, and drops back down when turned off.

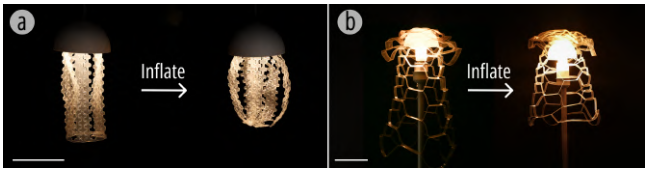

Figure 21: (a) Lamp constructed with "Bulging Waveform Surface" modules, showing a gravity-dependent drooping form when uninflated, and a stable outward-arching 3D shape upon inflation. (b) Lamp built with "Concentric Circular Slit" modules, transitioning from a loose mesh to a defined, saddle-like shape upon inflation. (Scale bar: 100 mm.)

6 Discussion, Limitation, and Future Work

6.1 Control of Electrostatic Adhesion

Our approach leverages the inherent electrostatic adhesion properties of the material, making it well-suited for thermal welding processes. The strength of electrostatic adhesion plays a significant role in performance. For instance, when small-sized inflatables are made from thin materials, inflation may cause them to overlap, and upon deflation, the electrostatic force may prevent the structure from returning to its original state due to the overlapping shrinkage. Moreover, thicker materials tend to weaken the electrostatic adhesion. To address this, we employed multi-layer thin films to achieve the desired level of electrostatic force. We also explored the use of low-cost electrostatic generators to enhance the adhesion of materials, such as TPU, that initially exhibit weak electrostatic properties.

6.2 Compatibility of Complex Inflatable Structure

The fabricating method proposed in this study offers significant advantages for producing high-precision small inflatables with slits or hollow structures and complex air channels. In addition to the Kirigami inflatable structure, which is the focus of this paper, our method is also applicable to other structures. As Figure 22 shows, our technique enables the fabrication of hollow patterns to create 3D shell-like surfaces (the fabrication file is adapted from research in computer graphics [30], with scaling adjustments). This manufacturing approach opens new possibilities for designing intricate internal patterns for inflatables. Future research on inflatable structures and their applications can benefit from the method we proposed.

6.3 Sensing Integration

Inflatables with sensing capability will improve the application in the HCI field [36]. Inspired by [44], we have explored methods for integrating sensing capabilities into the KiriInflate structure. The Kirigami design is particularly suitable for embedding circuits while maintaining their stability, and the inflation process introduces changes in the electrical properties. We conducted preliminary trials by applying graphene conductive spray paint onto the inflatables, achieving a sensing effect without compromising the deformation or mechanical performance of the inflatable. Specifically,

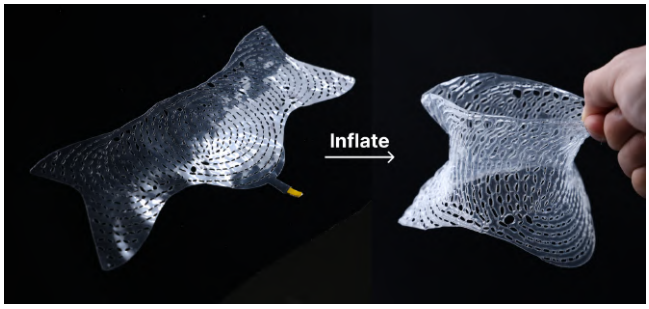

Figure 22: Fabrication outcome of a curved structure featuring a complex, small-scale hollow pattern. The fabrication pattern is adapted from [30].

the inflation process causes a reduction in resistance, while passive stretching results in an increase in resistance (Figure 23a). We included curves showing resistance changes under uninflated, inflated, and stretched conditions, measured using an Arduino-based setup (Figure 23b).

Further experiments are needed to assess whether this approach is suitable for miniaturized inflatables made from ultra-thin materials. Additionally, the proposed inflatable kirigami structures are well suited for conforming sensor arrays—such as electrodes [46]—to complex body surfaces while maintaining close skin contact. When integrated with functional circuits, these structures could enable various wearable applications in health monitoring and interactive systems. Moreover, the observed resistance changes may serve as feedback signals for closed-loop inflation control.

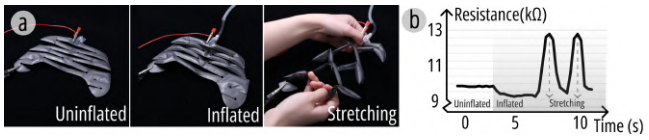

Figure 23: (a) Inflation and stretching applied to the game controller. (b) Resistance decreases during inflation and increases during stretching.

6.4 Comparison with Other Actuators

This section presents a quantitative comparison between KiriInflate and a representative existing kirigami-based inflatable actuator, Weld n'Cut [11], conducted under identical experimental conditions, with results summarized in Table 5. The data reveal that KiriInflate achieves a superior contraction ratio. We attribute this advantage to two key features: first, our fabrication process creates narrower seals that increase the effective air channel width for greater contraction; second, optimized round-hole slit ends promote more efficient stacking of the inflated units. Furthermore, our technique enables fabrication at significantly smaller scales (down to 0.1× the size of prior samples), a direct result of the precise alignment afforded by electrostatic adhesion. However, this performance profile involves a trade-off. Due to its PE film construction with lower pressure tolerance, KiriInflate produces a smaller actuation

force (≥ 32 g load) compared to more robust TPU-based actuators like Weld n'Cut (≥ 50 g load). Therefore, our method is ideally suited for applications that prioritize small scale, high compliance, and large deformation (both contraction and stretch), rather than high force output.

Table 5: Performance Comparison of Pneumatic Kirigami Actuators.

Method	Contraction Ratio	Force	Pressure Tolerance
Weld n'Cut [11]	40 %	≥ 50 g load	N/A (> 100 kPa)
KiriInflate	67.6%	≥ 32 g load	75 kPa

Note: Both methods were tested on samples with a scale of 150 mm × 125 mm. Contraction ratio and force values are measured at 50 kPa. The ratio is relative to the original length before inflation.

In the broader context of pneumatic actuators, KiriInflate demonstrates clear superiority in large-magnitude deformation. Its maximum contraction of 83.5% significantly exceeds that of both typical artificial muscles (55.3% [16] and McKibben actuators (32% [15]). This adaptability is rooted in the complex, cross-scale structures our method can produce, albeit with the trade-offs of lower pressure limits and actuation force. Thus, KiriInflate is ideally suited for applications prioritizing large, adaptable deformation over high force output.

6.5 Durability and Fatigue

6.5.1 Fabrication Consistency and Pressure Tolerance. To assess consistency of the fabrication method, we conducted inflation tests on KiriInflate basic structure with three distinct sizes: small (2 mm channel width, single-layer 0.03 mm thickness), medium (8 mm, 0.07 mm), and large (14 mm, 0.14 mm). Each group included ten samples. The tests showed no leakage in small samples and only one failure in both the medium and large samples. Analysis indicated that leakage mainly resulted from microbubbles trapped between film layers, which hindered full fusion.

The maximum pressure capacity was measured by inflating samples until failure, defined as the point at which continuous bubbles appeared in the water during inflation. The results showed a clear negative correlation between size and pressure resistance. Small samples had the highest tolerance, failing around 120 kPa (range: 80–220 kPa). All failures in this group resulted from inlet seal rupture rather than tearing of the air chamber, indicating that inlet sealing was the main limitation. Medium and large samples showed lower capacities (45–80 kPa and 45–60 kPa) and mainly failed due to tearing near pattern corners where stress concentration developed. To improve this, we explored whether reinforcing the structure with additional heat-seal boundaries could improve strength. We found that applying a triple heat-seal with 0.5 mm spacing increased the maximum pressure in large samples to 175 kPa, which confirmed that this method was effective.

6.5.2 Inflation Fatigue Testing. To evaluate durability under repeated inflation, we performed cyclic inflation tests on medium samples (8 mm channel width, single-layer 0.07 mm thickness). We applied cyclic loads of 50 kPa using a pneumatic pump, with 2 seconds inflation and 2 seconds deflation to simulate repeated use. Over a test duration of approximately 7 hours per sample, failures occurred after around 6,500 cycles in all three replicates. All failures initiated at a sharp corners, where stress concentration caused cumulative fatigue and rupture.

6.5.3 Tensile Fatigue Testing. As shown in Figure 24a, dynamic tensile fatigue tests were performed on pre-inflated (50 kPa) medium samples using a single-arm tensile tester (Xiamen Qunlong Instruments, QL-5W). Cyclic loading (10 mm/s) was applied over a 0–130 mm displacement range, with force–displacement recorded at 50 Hz.

After 200 cycles, samples remained intact without any physical damage. We observed that the force–displacement curves stayed stable during the first 60 cycles, with peak tensile force fluctuating around 2.82 N. After 60 cycles, the peak force began to decrease gradually. By the 100th cycle, peak force had dropped by 9.9% to approximately 2.54 N. At the 200th cycle, peak force had decreased by 25.9% to about 2.09 N, indicating gradual stiffness degradation following the initial stable phase. Force–displacement curves for cycles 0 to 20 and cycles 180 to 200 are shown in Figure 24b.

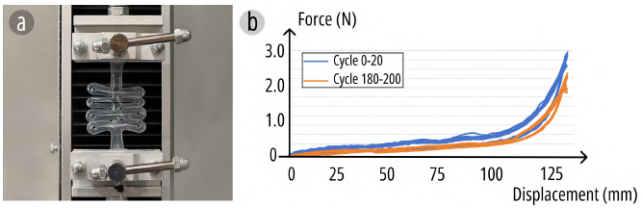

Figure 24: Tensile fatigue test. (a) Experimental setup. (b) Force-displacement curves comparing early and late cycles, showing stiffness degradation.

6.6 Simulation Challenges

Our online web tool currently provides basic parametric structure generation capabilities. However, developing an inflation process simulation and real-time deformation previews is a challenging task. This is primarily due to the complexity of the inflatable structure and the uncertainties of internal overlap and collision during inflation. Future work will further develop the tool to support simulation, real-time deformation previews, and design optimization.

7 Conclusion

In this study, we present KiriInflate, a novel fabrication method that enables rapid, high-resolution construction of inflatable structures with complex internal slit patterns. By leveraging the static cling of PE films and the dual cutting-welding capability of laser cutters, our approach enables high-resolution, single-step fabrication of intricately patterned inflatables across scales without requiring specialized hardware or alignment processes. This significantly lowers the technical barrier to producing high-resolution kirigami inflatables. Through a series of experiments, we summarize the laser parameter settings required to achieve (a) simultaneous heat

welding and cutting and (b) heat welding without cutting across materials of varying thicknesses. Considering the combined effects of the heat sealing pattern and slit geometry, we developed a structural library of Kirigami-based inflatable modules that exhibit diverse actuation behaviors and passive stretch capabilities. Through systematic experimentation, we examined how variables such as scale, geometric parameters, and film thickness influence actuation performance, including active contraction, passive stretchability, and force output. These empirical findings inform the development of a parametric design tool that enables users to customize inflatable structures. We demonstrate the versatility and applicability of this approach through four examples: (1) an eyelid-lifting assistive wearable that accommodates natural blinking; (2) a dynamic elbow brace; (3) a game controller that integrates inflation-driven haptic feedback with passive stretch interactions; and (4) a collection of shape-reconfigurable lamps. These applications illustrate the potential of the KiriInflate system in achieving dynamic conformability, shape reconfiguration, and haptic feedback for tangible interaction. Looking forward, we envision KiriInflate unlocking new opportunities for designers, makers, and researchers to leverage the art of slits in inflatables for creating interactive experiences across a wide range of scales and application scenarios.

Acknowledgements

This project was supported by the National Natural Science Foundation of China under Grant No. T2422021, and by Zhejiang Provincial Natural Science Foundation of China under Grant No. LY23F020020. We would like to express our sincere gratitude to Prof. Lining Yao, David Jourdan, Yuecheng Peng, and Qiuyu Lu for their insightful contributions during the early-stage discussions of this project. We also thank Jeremy Chen for his efforts on the initial fabrication attempts. We are grateful to Yingying Ren, Prof. Julian Panetta, and Florin Isvoranu for generously sharing their fabrication files and manufacturing expertise related to their former work. Special thanks are extended to Junzhe Ji and Chao Yuan for their invaluable help and guidance on the parametric generation of structures and their corresponding simulation trials.

References

[1] ProByLas AG. [n. d.]. Optics Ball Contour Process - Local Clamping. https://www.probylas.com/en/technology/weldingprocess/contour/ball/

[2] Matteo Alberghini, Seongdon Hong, L. Marcelo Lozano, Volodymyr Korolovych, Yi Huang, Francesco Signorato, S. Hadi Zandavi, Corey Fucetola, Ihsan Uluturk, Michael Y. Tolstorukov, Gang Chen, Pietro Asinari, Richard M. Osgood, Matteo Fasano, and Svetlana V. Boriskina. 2021. Sustainable polyethylene fabrics with engineered moisture transport for passive cooling. *Nature Sustainability* 4, 8 (March 2021), 715–724. doi:10.1038/s41893-021-00688-5 Publisher: Springer Science and Business Media LLC.

[3] Anne Katherine Brooks, Sudesna Chakravarty, Maryam Ali, and Vamsi K Yadavalli. 2022. Kirigami-Inspired Biodesign for Applications in Healthcare. *Advanced Materials* 34, 18 (May 2022), 2109550. doi:10.1002/adma.202109550

[4] Zekun Chang, Tung D. Ta, Koya Narumi, Heeju Kim, Fuminori Okuya, Dongchi Li, Kunihiro Kato, Jie Qi, Yoshinobu Miyamoto, Kazuya Saito, and Yoshihiro Kawahara. 2020. Kirigami Haptic Swatches: Design Methods for Cut-and-Fold Haptic Feedback Mechanisms. In *Proceedings of the 2020 CHI Conference on Human Factors in Computing Systems (CHI '20)*. Association for Computing Machinery, New York, NY, USA, 1–12. doi:10.1145/3313831.3376655

[5] S.H. Chen, K.C. Chan, D.X. Han, L. Zhao, and F.F. Wu. 2019. Programmable super elastic kirigami metallic glasses. *Materials & Design* 169 (May 2019), 107687. doi:10.1016/j.matdes.2019.107687

[6] Kyung Yun Choi and Hiroshi Ishii. 2021. Therms-Up!: DIY Inflatables and Interactive Materials by Upcycling Wasted Thermoplastic Bags. In *Proceedings of the Fifteenth International Conference on Tangible, Embedded, and Embodied Interaction*. ACM, Salzburg Austria, 1–8. doi:10.1145/3430524.3442457

[7] Sewoong Chung, Altair Coutinho, and Hugo Rodrigue. 2023. Manufacturing and Design of Inflatable Kirigami Actuators. *IEEE Robotics and Automation Letters* 8, 1 (Jan. 2023), 25–32. doi:10.1109/LRA.2022.3221318

[8] Alexandra Delazio, Ken Nakagaki, Roberta L. Klatzky, Scott E. Hudson, Jill Fain Lehman, and Alanson P. Sample. 2018. Force Jacket: Pneumatically-Actuated Jacket for Embodied Haptic Experiences. In *Proceedings of the 2018 CHI Conference on Human Factors in Computing Systems*. ACM, Montreal QC Canada, 1–12. doi:10.1145/3173574.3173894

[9] Josef Finsterer. 2003. Ptosis: Causes, Presentation, and Management. *Aesthetic Plastic Surgery* 27, 3 (June 2003), 193–204. doi:10.1007/s00266-003-0127-5

[10] Tian Gao, Emmanuel Siéfert, Antonio DeSimone, and Benoît Roman. 2020. Shape Programming by Modulating Actuation over Hierarchical Length Scales. *Advanced Materials* 32, 47 (Nov. 2020), 2004515. doi:10.1002/adma.202004515

[11] Arman Goshtasbi, Burcu Seyidoğlu, Saravana Prashanth Murali Babu, Aida Parvaresh, Cao Danh Do, and Ahmad Rafsanjani. 2025. Weld n'Cut: Automated fabrication of inflatable fabric actuators. In *2025 IEEE 8th International Conference on Soft Robotics (RoboSoft)*. IEEE, Lausanne, Switzerland, 1–6. doi:10.1109/robosoft63089.2025.11020948

[12] Daniel Groeger and Jürgen Steimle. 2019. LASEC: Instant Fabrication of Stretchable Circuits Using a Laser Cutter. In *Proceedings of the 2019 CHI Conference on Human Factors in Computing Systems*. ACM, Glasgow Scotland Uk, 1–14. doi:10.1145/3290605.3300929

[13] Sheng-Pei Hu and June-Hao Hou. 2019. Pneu-Multi-Tools: Auto-Folding and Multi-Shapes Interface by Pneumatics in Virtual Reality. In *The Adjunct Publication of the 32nd Annual ACM Symposium on User Interface Software and Technology*. ACM, New Orleans LA USA, 36–38. doi:10.1145/3332167.3357107

[14] Lishuai Jin, Antonio Elia Forte, Bolei Deng, Ahmad Rafsanjani, and Katia Bertoldi. 2020. Kirigami-Inspired Inflatables with Programmable Shapes. *Advanced Materials* 32, 33 (Aug. 2020), 2001863. doi:10.1002/adma.202001863

[15] Ozgun Kilic Afsar, Ali Shtarbanov, Hila Mor, Ken Nakagaki, Jack Forman, Karen Modrei, Seung Hee Jeong, Klas Hjort, Kristina Höök, and Hiroshi Ishii. 2021. OmniFiber: Integrated Fluidic Fiber Actuators for Weaving Movement based Interactions into the 'Fabric of Everyday Life'. In *The 34th Annual ACM Symposium on User Interface Software and Technology*. ACM, Virtual Event USA, 1010–1026. doi:10.1145/3472749.3474802

[16] Junghan Kwon, Sohee John Yoon, and Yong-Lae Park. 2020. Flat Inflatable Artificial Muscles With Large Stroke and Adjustable Force– Length Relations. *IEEE Transactions on Robotics* 36, 3 (June 2020), 743–756. doi:10.1109/tro.2019.2961300 Publisher: Institute of Electrical and Electronics Engineers (IEEE).

[17] Qiuyu Lu, Jifei Ou, João Wilbert, André Haben, Haipeng Mi, and Hiroshi Ishii. 2019. milliMorph – Fluid-Driven Thin Film Shape-Change Materials for Interaction Design. In *Proceedings of the 32nd Annual ACM Symposium on User Interface Software and Technology*. ACM, New Orleans LA USA, 663–672. doi:10.1145/3332165.3347956

[18] Yiyue Luo, Kui Wu, Andrew Spielberg, Michael Foshey, Daniela Rus, Tomás Palacios, and Wojciech Matusik. 2022. Digital Fabrication of Pneumatic Actuators with Integrated Sensing by Machine Knitting. In *CHI Conference on Human Factors in Computing Systems*. ACM, New Orleans LA USA, 1–13. doi:10.1145/3491102.3517577

[19] Yusuke Morikawa, Shota Yamagiwa, Hirohito Sawahata, Rika Numano, Kowa Koida, and Takeshi Kawano. 2019. Stretchable Devices: Donut-Shaped Stretchable Kirigami: Enabling Electronics to Integrate with the Deformable Muscle (Adv. Healthcare Mater. 23/2019). *Advanced Healthcare Materials* 8, 23 (Dec. 2019), 1970092. doi:10.1002/adhm.201970092

[20] Takafumi Morita, Ziyuan Jiang, Kanon Aoyama, Ayato Minaminosono, Yu Kuwajima, Naoki Hosoya, Shingo Maeda, and Yasuaki Kakehi. 2023. InflatableMod: Untethered and Reconfigurable Inflatable Modules for Tabletop-sized Pneumatic Physical Interfaces. In *Proceedings of the 2023 CHI Conference on Human Factors in Computing Systems*. ACM, Hamburg Germany, 1–15. doi:10.1145/3544548.3581353

[21] Stefanie Mueller, Bastian Kruck, and Patrick Baudisch. 2013. LaserOrigami: laser-cutting 3D objects. In *Proceedings of the SIGCHI Conference on Human Factors in Computing Systems*. ACM, Paris France, 2585–2592. doi:10.1145/2470654.2481358

[22] Takumi Murayama, Junichi Yamaoka, and Yasuaki Kakehi. 2020. Reflatables: A Tube-based Reconfigurable Fabrication of Inflatable 3D Objects. In *Extended Abstracts of the 2020 CHI Conference on Human Factors in Computing Systems*. ACM, Honolulu HI USA, 1–8. doi:10.1145/3334480.3382904

[23] Benigno Muñoz-Barron, X. Yamile Sandoval-Castro, Eduardo Castillo-Castaneda, and Med Amine Laribi. 2024. Characterization of a Rectangular-Cut Kirigami Pattern for Soft Material Tuning. *Applied Sciences* 14, 8 (April 2024), 3223. doi:10.3390/app14083223

[24] Tom Nardi. 2019. Custom Inflatables Are Only A Laser Beam Away. https://hackaday.com/2019/04/02/custom-inflatables-are-only-a-laser-beam-away/

[25] Ryuma Niiyama, Young Ah Seong, Yoshihiro Kawahara, and Yasuo Kuniyoshi. 2021. Blower-Powered Soft Inflatable Joints for Physical Human-Robot Interaction. *Frontiers in Robotics and AI* 8 (Aug. 2021), 720683. doi:10.3389/frobt.2021.

720683

[26] Sora Oka, Kazuki Koyama, Tomoyuki Gondo, Yasushi Ikeda, Yoshihiro Kawahara, and Koya Narumi. 2025. Pneumatic Laser Origami: Rapid and Large-Scale Fabrication of Laser-Welded Pouch Motors for Shape-Changing Products. In *Proceedings of the Nineteenth International Conference on Tangible, Embedded, and Embodied Interaction*. ACM, Bordeaux/Talence France, 1–12. doi:10.1145/3689050.3704956

[27] Jifei Ou, Mélina Skouras, Nikolaos Vlavianos, Felix Heibeck, Chin-Yi Cheng, Jannik Peters, and Hiroshi Ishii. 2016. aeroMorph - Heat-sealing Inflatable Shape-change Materials for Interaction Design. In *Proceedings of the 29th Annual Symposium on User Interface Software and Technology*. ACM, Tokyo Japan, 121–132. doi:10.1145/2984511.2984520

[28] Julian Panetta, Florin Isvoranu, Tian Chen, Emmanuel Siéfert, Benoît Roman, and Mark Pauly. 2021. Computational inverse design of surface-based inflatables. *ACM Transactions on Graphics* 40, 4 (Aug. 2021), 1–14. doi:10.1145/3450626.3459789

[29] Lukas Rambold, Robert Kovacs, Conrad Lempert, Muhammad Abdullah, Helena Lendowski, Lukas Fritzsche, Martin Taraz, and Patrick Baudisch. 2023. AirTied: Automatic Personal Fabrication of Truss Structures. In *Proceedings of the 36th Annual ACM Symposium on User Interface Software and Technology*. ACM, San Francisco CA USA, 1–10. doi:10.1145/3586183.3606820

[30] Yingying Ren, Julian Panetta, Seiichi Suzuki, Uday Kusupati, Florin Isvoranu, and Mark Pauly. 2024. Computational Homogenization for Inverse Design of Surface-based Inflatables. *ACM Transactions on Graphics* 43, 4 (July 2024), 1–18. doi:10.1145/3658125

[31] Harpreet Sareen, Udayan Umapathi, Patrick Shin, Yasuaki Kakehi, Jifei Ou, Hiroshi Ishii, and Pattie Maes. 2017. Printflatables: Printing Human-Scale, Functional and Dynamic Inflatable Objects. In *Proceedings of the 2017 CHI Conference on Human Factors in Computing Systems*. ACM, Denver Colorado USA, 3669–3680. doi:10.1145/3025453.3025898

[32] Burcu Seyidoğlu, Aida Parvaresh, Bahman Taherkhani, and Ahmad Rafsanjani. 2025. Inflatable Kirigami Crawlers. *Advanced Robotics Research* (June 2025). doi:10.1002/adrr.202500044

[33] Rachel A. Shveda, Anoop Rajappan, Te Faye Yap, Zhen Liu, Marquise D. Bell, Barclay Jumet, Vanessa Sanchez, and Daniel J. Preston. 2022. A wearable textile-based pneumatic energy harvesting system for assistive robotics. *Science Advances* 8, 34 (Aug. 2022), eabo2418. doi:10.1126/sciadv.abo2418

[34] Emmanuel Siéfert, Etienne Reyssat, José Bico, and Benoît Roman. 2019. Programming curvilinear paths of flat inflatables. *Proceedings of the National Academy of Sciences* 116, 34 (Aug. 2019), 16692–16696. doi:10.1073/pnas.1904544116

[35] Yue Sun, Wangjie Ye, Yao Chen, Weiying Fan, Jian Feng, and Pooya Sareh. 2021. Geometric design classification of kirigami-inspired metastructures and metamaterials. *Structures* 33 (Oct. 2021), 3633–3643. doi:10.1016/j.istruc.2021.06.072

[36] Saiganesh Swaminathan, Michael Rivera, Runchang Kang, Zheng Luo, Kadri Bugra Ozutemiz, and Scott E. Hudson. 2019. Input, Output and Construction Methods for Custom Fabrication of Room-Scale Deployable Pneumatic Structures. *Proceedings of the ACM on Interactive, Mobile, Wearable and Ubiquitous Technologies* 3, 2 (June 2019), 1–17. doi:10.1145/3328933

[37] Shan-Yuan Teng, Tzu-Sheng Kuo, Chi Wang, Chi-huan Chiang, Da-Yuan Huang, Liwei Chan, and Bing-Yu Chen. 2018. PuPoP: Pop-up Prop on Palm for Virtual Reality. In *Proceedings of the 31st Annual ACM Symposium on User Interface Software and Technology*. ACM, Berlin Germany, 5–17. doi:10.1145/3242587.3242628

[38] Shan-Yuan Teng, Cheng-Lung Lin, Chi-huan Chiang, Tzu-Sheng Kuo, Liwei Chan, Da-Yuan Huang, and Bing-Yu Chen. 2019. TilePoP: Tile-type Pop-up Prop for Virtual Reality. In *Proceedings of the 32nd Annual ACM Symposium on User Interface Software and Technology*. ACM, New Orleans LA USA, 639–649. doi:10.1145/3332165.3347958

[39] Udayan Umapathi, Hsiang-Ting Chen, Stefanie Mueller, Ludwig Wall, Anna Seufert, and Patrick Baudisch. 2015. LaserStacker: Fabricating 3D Objects by Laser Cutting and Welding. In *Proceedings of the 28th Annual ACM Symposium on User Interface Software & Technology*. ACM, Charlotte NC USA, 575–582. doi:10.1145/2807442.2807512

[40] Guanyun Wang, Yue Yang, Mengyan Guo, Kuangqi Zhu, Zihan Yan, Qiang Cui, Zihong Zhou, Junzhe Ji, Jiaji Li, Danli Luo, and others. 2023. ThermoFit: Thermoforming smart orthoses via metamaterial structures for body-fitting and component-adjusting. *Proceedings of the ACM on Interactive, Mobile, Wearable and Ubiquitous Technologies* 7, 1 (2023), 1–27. Publisher: ACM New York, NY, USA.

[41] Junichi Yamaoka, Kazunori Nozawa, Shion Asada, Ryuma Niiyama, Yoshihiro Kawahara, and Yasuaki Kakehi. 2018. AccordionFab: Fabricating Inflatable 3D Objects by Laser Cutting and Welding Multi-Layered Sheets. In *Adjunct Proceedings of the 31st Annual ACM Symposium on User Interface Software and Technology*. ACM, Berlin Germany, 160–162. doi:10.1145/3266037.3271636

[42] Zeyu Yan, Anup Sathya, Sahra Yusuf, Jyh-Ming Lien, and Huaishu Peng. 2022. Fibercuit: Prototyping High-Resolution Flexible and Kirigami Circuits with a Fiber Laser Engraver. In *The 35th Annual ACM Symposium on User Interface Software and Technology*. ACM, Bend OR USA, 1–13. doi:10.1145/3526113.3545652

[43] Yue Yang, Lei Ren, Chuang Chen, Bin Hu, Zhuoyi Zhang, Xinyan Li, Yanchen Shen, Kuangqi Zhu, Junzhe Ji, Yuyang Zhang, Yongbo Ni, Jiayi Wu, Qi Wang, Jiang Wu, Lingyun Sun, Ye Tao, and Guanyun Wang. 2024. SnapInflatables: Designing Inflatables with Snap-through Instability for Responsive Interaction. In *Proceedings of the CHI Conference on Human Factors in Computing Systems*. ACM, Honolulu HI USA, 1–15. doi:10.1145/3613904.3642933

[44] Clement Zheng, HyunJoo Oh, Laura Devendorf, and Ellen Yi-Luen Do. 2019. Sensing Kirigami. In *Proceedings of the 2019 on Designing Interactive Systems Conference (DIS '19)*. Association for Computing Machinery, New York, NY, USA, 921–934. doi:10.1145/3322276.3323689

[45] Yu Meng Zhou, Cameron J. Hohimer, Harrison T. Young, Connor M. McCann, David Pont-Esteban, Umut S. Civici, Yichu Jin, Patrick Murphy, Diana Wagner, Tazzy Cole, Nathan Phipps, Haedo Cho, Franchesco Bertacchi, Isabella Pignataro, Tommaso Proietti, and Conor J. Walsh. 2024. A portable inflatable soft wearable robot to assist the shoulder during industrial work. *Science Robotics* 9, 91 (June 2024), eadi2377. doi:10.1126/scirobotics.adi2377

[46] Junyi Zhu, Jackson C Snowden, Joshua Verdejo, Emily Chen, Paul Zhang, Hamid Ghaednia, Joseph H Schwab, and Stefanie Mueller. 2021. EIT-Kit: An Electrical Impedance Tomography Toolkit for Health and Motion Sensing. In *The 34th Annual ACM Symposium on User Interface Software and Technology (UIST '21)*. Association for Computing Machinery, New York, NY, USA, 400–413. doi:10.1145/3472749.3474758 event-place: Virtual Event, USA.